Weinberger, R. Javid, B. Lepan, *Proc. Natl. Acad. Sci. U.S.A.* **90**, 2394 (1993).
5. M. W. Pettet and C. D. Gilbert, *Proc. Natl. Acad. Sci. U.S.A.* **89**, 8366 (1992).
6. C. D. Salzman, C. M. Murasugi, K. H. Britten, W. T. Newsome, *J. Neurosci.* **12**, 2331 (1992); C. M. Murasugi, C. D. Salzman, W. T. Newsome, *ibid.* **13**, 1719 (1993).
7. The responses of single neurons were recorded while the monkey performed the direction discrimination task. In each experiment, we placed the stimulus so that it matched the size and location of the neuron's receptive field, and we adjusted the speed of the coherently moving dots to elicit an optimal response from the neuron. The motion signal was presented either in the cell's preferred direction or in the opposite (null) direction. In an individual trial, the monkey was required to fixate a stationary point of light for 2 s while the stimulus was presented. After the viewing period, the monkey indicated his judgment by making a saccadic eye movement to one of two light-emitting diodes corresponding to the two possible directions of motion. Eye movements were measured continuously with the scleral search coil technique [D. A. Robinson, *IEEE Trans. Biomed. Eng.* **10**, 137 (1963)]. The monkey received a liquid reward for a correct choice. Incorrect choices were punished by a brief time-out period. If the monkey broke fixation prematurely, the trial was aborted and the data discarded. Cells were included in our data sample on the basis of direction selectivity—we required that their responses to strong motion in the null direction be consistently smaller than their responses to strong motion in the preferred direction. For most cells, the response in the null direction was equal to or less than the spontaneous firing rate.
8. K. H. Britten, M. N. Shadlen, W. T. Newsome, J. A. Movshon, *J. Neurosci.* **12**, 4745 (1992).
9. The average neuronal threshold ratio in the untrained monkey was 0.79, corresponding to an increase in neuronal sensitivity of 26.4%. The difference in thresholds measured in the first and second blocks of trials was statistically significant (paired t test, $P = 0.005$, df = 25). Although the mean threshold ratio was lower for neurons recorded in the untrained monkey than for those recorded in the trained monkeys, the overall distributions of threshold ratios were not significantly different for the two groups (unpaired t test, $P = 0.15$, df = 226).
10. In general, enhanced discriminative capacity of single neurons can result either from changes in neuronal responsiveness or from a decrease in response variability. An analysis of our data supports the first possibility. We assessed the change in responsiveness by measuring, for each neuron, the slope of the response function relating motion coherence level to firing rate. Slopes were computed separately for the preferred and null direction response functions in each block of trials. These correlation-response functions were fitted well by straight lines for roughly half of the MT neurons [K. H. Britten, M. N. Shadlen, W. T. Newsome, J. A. Movshon, *Visual Neurosci.* **8**, 1157 (1993)], and this analysis was done only on these cells. The slopes of the coherence-response functions for preferred-direction motion were significantly steeper in the second block of trials, which indicated increased responsiveness (paired t test, $P < 0.0002$, df = 151). Across coherence levels, firing rates in response to preferred-direction motion increased by an average of 6.6% in the second block of trials. The slopes of the null direction coherence-response functions were significantly more negative, on average, in the second block of trials (paired t test, $P < 0.0001$, df = 116). Response variance, normalized for firing rate, was unchanged between the first and second blocks of trials.
11. We did an analysis of covariance to determine whether the composite neuronal and psychometric thresholds depended on stimulus repetition number in the same fashion. We used an interaction term between stimulus repetition number and data set (psychophysical or neuronal) to test the null hypothesis that the two data sets were fit as well with the same as with different slopes. The interaction term was not significant ($P = 0.17$).
12. D. Y. Ts'o, C. D. Gilbert, T. N. Wiesel, *J. Neurosci.* **6**, 1160 (1986).
13. M. Ahissar and S. Hochstein, *Proc. Natl. Acad. Sci. U.S.A.* **90**, 5718 (1993); K. Ball and R. Sekular, *Vision Res.* **27**, 953 (1987); N. Berardi and A. Fiorentini, *J. Physiol.* **384**, 633 (1987); A. Karni and D. Sagi, *Proc. Natl. Acad. Sci. U.S.A.* **88**, 4966 (1991); T. Poggio, M. Fahle, S. Edelman, *Science* **256**, 1018 (1992).
14. R. F. Quick, *Kybernetik* **16**, 65 (1974).
15. We thank M. N. Shadlen for suggesting the time course analysis, C. Koch for helpful suggestions during the course of this work, C. D. Salzman for useful comments on the manuscript, and J. Stein for excellent technical assistance. Supported by the National Eye Institute and by training fellowships from the McDonnel-Pew program in cognitive neuroscience and the CNRS of France.

22 September 1993; accepted 7 January 1994

Global Form and Singularity: Modeling the Blind Spot's Role in Lateral Geniculate Morphogenesis

Daeyeol Lee and Joseph G. Malpeli*

Optic nerve terminals segregate by functional class into distinct layers in the lateral geniculate nucleus, the thalamic relay nucleus of the visual system. In the rhesus monkey, the number of geniculate layers changes abruptly from six posteriorly (central vision) to four anteriorly (peripheral vision). The plane of transition between these patterns passes through small laminar gaps corresponding to the perceptual blind spot caused by the exit of the optic nerve from the eyeball. However, this plane of transition has no apparent functional link to the blind spot. A thermodynamic model of geniculate morphogenesis supports the hypothesis that the blind spot traps the transition in its stereotypic position by introducing a singularity in an otherwise smooth gradient in forces guiding the development of geniculate morphogenesis. This relation suggests that small-scale anomalies may be important in the determination of large-scale patterns in biological structure.

Although brain morphology is subject to considerable individual differences, certain features are constant. For example, there are substantial variations in the size, position, and orientation of the rhesus lateral geniculate nucleus (LGN), the thalamic relay nucleus interposed between the eye and cerebral cortex. However, the internal laminar structure of the LGN maintains an invariant relation with a seemingly unrelated feature, the blind spot caused by the optic nerve exiting the eyeball through the optic disk. Geniculate retinotopy is so precise that the blind spot is represented by small gaps free of relay cells (optic disk gaps). These gaps lie in the plane of transition separating a six-layered posterior region (representing central vision) from a four-layered anterior region (peripheral binocular vision) (*1–3*). This association between the transition and gaps is puzzling: Many psychophysical and anatomical aspects of vision vary dramatically with retinal eccentricity, but the most rapid changes occur at eccentricities well within that of the optic disk. Furthermore, there is no evidence of sudden changes in any perceptual function at the transition and no apparent reason why any such changes should be associated with the blind spot. Here we consider this problem from a developmental viewpoint. We suggest that the blind spot traps the transition at its stereotypic location by introducing a singularity in a gradient controlling laminar development. To evaluate this proposition, we developed a thermodynamic model of geniculate morphogenesis, in which a realistic laminar transition is induced by an anteroposterior gradient in interaction forces between terminals. We then examined the effects of the optic disk gaps on the position of this transition using simulated annealing.

Our simulation was confined to the plane of symmetry of the LGN: a roughly rectangular surface dividing the nucleus into medial and lateral halves. This plane represents the horizontal meridian, so retinotopic organization is described by a single coordinate, eccentricity. Axon terminals from two "retinae" were categorized into six groups according to eye (ipsilateral or contralateral), major functional class (M or P) (*4*), and (for P cells) polarity of receptive-field center (On or Off). The density of retinal cells dropped with eccentricity, paralleling the number of geniculate cells per unit area of visual space (*5*). Because in normal development the formation of layers is induced by the arrival of retinal axons (*6*) and the main functional properties of geniculate relay cells mirror those of their retinal afferents, we considered only the distribu-

D. Lee, Neuroscience Program, University of Illinois, 603 East Daniel Street, Champaign, IL 61820, USA.
J. G. Malpeli, Department of Psychology, University of Illinois, 603 East Daniel Street, Champaign, IL 61820, USA.

*To whom correspondence should be addressed.

tion of retinal terminals in our model.

In simulated annealing, the likelihood that a system resides in a certain configuration is defined in terms of an energy function, with lower energy corresponding to more favorable states. The goal is to move systems to global energy minima through iterative procedures (*7*). We defined a retinal terminal's energy as a sum of several independent energy functions. Some functions depended on spatial position, favoring a particular dorsoventral position for each of the six groups of terminals (*8*). Other functions were correlational, favoring the close spacing of terminals of the same type and discouraging the close spacing of terminals of the opposite type. Correlational energies varied as Gaussian functions of interterminal distance, and the widths of these Gaussians (interaction distances) increased with eccentricity (overall, by a factor of 2.5). Terminal packing density was controlled by a correlational function that discourages the very close spacing of terminals, regardless of type.

Each point in visual space is represented in the LGN by a "projection column" that tends to cross layers perpendicularly (*2*, *9*). Projection columns were modeled by groups of six terminals sharing the same eccentricity, each from one of six functional groups defined above. We reduced local retinotopic scatter by assigning low energy to a terminal if its anteroposterior position was close to the mean terminal position in its column. Other types of correlational energies promoted global retinotopy.

The blind spot was represented by neutral ghost P-On and M terminals (characteristic of layers 6 and 1, respectively) from retinal ganglion cells in a small patch of retina in the contralateral eye. These terminals were subject to energies related to dorsoventral position in the LGN, retinotopy, and packing density but not to those related to functional type (M/P), eye, or center polarity (*10*). Terminals of the P-Off type (characteristic of layer 4) were entirely absent from this segment.

At the onset of the simulation, terminals were randomly distributed in a dorsoventral direction but were given a rough anteroposterior retinotopy to fix the representation of the fovea in the posterior part of the LGN. A terminal was randomly chosen, and its energy was calculated. It was then given a trial move in a random direction with a Gaussian probability distribution of distances, and the change in energy (ΔE) was calculated. For $\Delta E \leq 0$, the terminal was left in the new location. For $\Delta E > 0$, the terminal was either left in the new location, with a probability of $\exp(-\Delta E/T_N)$ (T_N is the "temperature" of the system for the Nth iteration), or returned to the old location (*11*). A single iteration consisted of a repetition of this procedure for every terminal in pseudorandom order. Initially, the temperature was set high enough that at least 60% of terminals moved to new positions. It was lowered geometrically for subsequent iterations ($T_{N+1} = 0.985T_N$), gradually "freezing" the nucleus into a low-energy state.

The key factor in the induction of proper laminar transitions is an anteroposterior gradient in interaction distances for correlational energies. Positional energies favor the six-layer pattern, whereas correlational energies favor the four-layer pattern, because correlational energies related to the eye of origin contribute more than those related to center polarity. As interaction distances increase, correlational energies gain importance relative to positional energies (*12*). We have not defined biological correlates of interaction distances, but it is reasonable to speculate that they are related to distances between neighboring cells or terminals (*13*).

For simulations without a blind spot, clean transitions between six and four layers formed at positions scattered over the posterior half of the nucleus (Figs. 1, A and B, and 2). When a blind spot was added to a simulation, most laminar transitions coincided with optic disk gaps (Figs. 1C and 2). With capture defined as a transition location within 4% of the length of the nucleus (approximately half the width of the optic disk gaps) from the gaps' center, the capture rate was 56.5% overall and 89% for the central 4 of the 12 positions tested (*14*). For all locations, the gaps swept up transitions within a total range equal to about one-fourth the length of the nucleus (the void around the line of successful captures in Fig. 2). Thus, if the "natural" (that is, without optic disk) position of the transition were close to the position of the real optic disk gaps, the gaps would always capture the transition (*15*, *16*).

These results suggest that the stereotypic form and location of the laminar transition arose as a developmental epiphenomenon resulting from a local singularity that breaks up an otherwise smooth developmental gradient. However, this hypothesis should not be taken to mean that the different laminar patterns are without functional consequence. There is no a priori reason why the brain could not have evolved to make use of this difference, regardless of how it first became established.

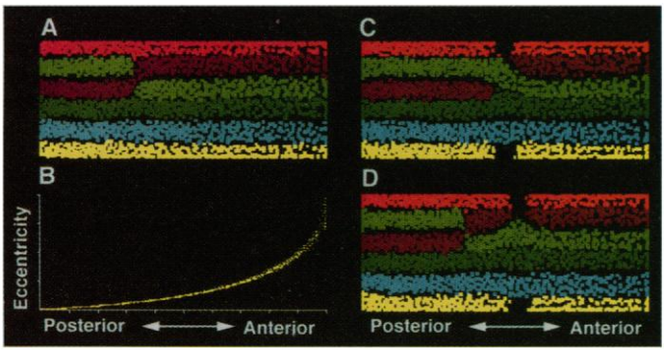

Fig. 1. Representative simulations of geniculate layers after 300 iterations. Conventionally, layers in the posterior LGN are numbered 1 to 6, ventral to dorsal: 1, contralateral-magnocellular (yellow); 2, ipsilateral-magnocellular (blue); 3, ipsilateral-parvocellular-Off (dark green); 4, contralateral-parvocellular-Off (dark red); 5, ipsilateral-parvocellular-On (light green); 6, contralateral-parvocellular-On (light red). The transition consists simply of a reversal in the relative positions of layers 4 and 5, resulting in the merger of parvocellular layers of the same eye anteriorly. The monocular crescent, which is represented at the anterior pole by one parvocellular and one magnocellular layer, is not included in these simulations. (**A**) Laminar transition in the absence of a blind spot. (**B**) Eccentricity of each terminal in (A). (**C**) Successful capture of laminar transition by optic disk gaps. (**D**) Failure of gaps to capture the transition.

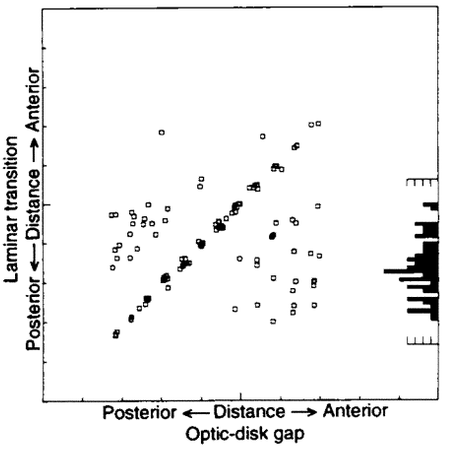

Fig. 2. Effects of optic disk gaps on laminar transition. The squares represent the location of optic disk gaps and laminar transition (determined analytically) for nine simulations at each of 12 positions of the blind spot chosen to span roughly the range of transitions occurring in the absence of a blind spot. Each axis spans the length of the LGN; each square represents one simulation. Squares along the main diagonal represent successful captures. Empty zones to either side of the diagonal show the "reach" of optic disk gaps in trapping transitions. The histogram represents the locations of laminar transitions in the absence of a blind spot (67 simulations).

Although gradients are commonly evoked as guiding forces in morphogenesis, the precipitation of a state change within a brain nucleus by a hole-like singularity may be an unusual event. However, the concepts employed in the present analysis can be broadened to include other types of morphological features (such as folds in extended sheets or boundaries between different structures) or other types of singularities (such as abrupt changes in the slope of a gradient). For example, the location of the occipital-parietal sulcus might be stabilized by perturbations at the posterior edge of the corpus callosum in energy functions related to the paths of corticocortical or corticothalamic fibers. In evaluating these possibilities, one may be able to draw on formal analyses of similar phenomena in the physical sciences, such as the induction of phase transitions by seed crystals or the propagation of crystalline dislocations from inclusions. One can only speculate about applying these ideas to other biological structures, but it is unusual to find only a single expression of a principle in nature.

Parameters of the model follow: The model's spatial dimensions are 100 (anteroposterior, horizontal) by 40 (dorsoventral, vertical) arbitrary units, and geniculate distances are expressed in these units. A total of 2400 terminals are grouped into 400 projection columns, numbered 1 to 400, from fovea to periphery. Within each projection column, an individual terminal is numbered according to lamination pattern in the posterior region of the nucleus (Fig. 1). Each terminal is assigned a retinal eccentricity (0 to 100 arbitrary units) by the following function:

$$e_k = 4.98\{\log[1388/(414 - k)]\}^{2.01} - 7.3$$

where e_k is the eccentricity and k is the projection column number. The optic disk spans 30 projection columns.

The total energy of a terminal of functional group g, having horizontal position x, vertical position y, eccentricity e, and residing in column k is

$$E_{\text{Total}} = E_{\text{Ret}} + E_{\text{Corr}} + E_{\text{Pos}}$$

where E_{Ret} establishes retinotopy and E_{Corr} and E_{Pos} are the respective correlational and positional energy functions related to laminar pattern.

$$E_{\text{Ret}} = G_1(x - \bar{x}_k) + \sum_{j \in J} G_2(\bar{x}_k - \bar{x}_j) + \sum_{w \in W} \{G_3(x_w - x)[G_4(e_w - e) + G_5(e_w - e)]\} + 150 \cdot S^-$$

where $\bar{x}_j$ is the mean horizontal position of terminals in column j and e_w and x_w are the eccentricity and horizontal position, respectively, of terminal w. The term J represents the set of all projection columns and W is the set of all terminals.

$$G_i(u) = A_i \exp\{-u^2/[s_i\Phi_i(k)]^2\}$$

for $i = 1, 2, 3, 4, 5$, where $\Phi_i(k)$ [and $\Phi(k)$, below] are scaling factors for interaction distances. The expression $\Phi_i(k) = 1$ for $i = 4$ or 5, and $0.0015k + 0.4$ otherwise. The value of $A_1 = -1500$, $s_1 = 8$; $A_2 = 150$, $s_2 = 4$; $A_3 = 1$, $s_3 = 6$; $A_4 = -10$, $s_4 = 8$; $A_5 = 4$, $s_5 = 20$. The term S^- is the number of ordinal inversions in mean horizontal position for all pairings of projection columns [$S^- = \frac{1}{2}\binom{400}{2}(1 - \tau)$, where τ is Kendall's τ between j and $\bar{x}_j$].

$$E_{\text{Corr}} = \sum_{w \in W} G_{\text{Space}}(d_w) + \sum_{w \in W_1} G_{\text{M/P}}(d_w) + \sum_{w \in W_2'} G_{\text{Pol,same}}(d_w) + \sum_{w \in W_2''} G_{\text{Pol,diff}}(d_w) + \sum_{w \in W_3'} G_{\text{Eye,same}}(d_w) + \sum_{w \in W_3''} G_{\text{Eye,diff}}(d_w)$$

where d_w is the distance between terminal w and the terminal in question. The term W is the same as above, W_1 is the set of all terminals of opposite cell type (M or P) to that of the given terminal, W_2' (W_2'') is the set of all terminals whose center polarity is the same as (different from) that of the given terminal, and W_3' (W_3'') is the set of all terminals whose eye of origin is the same as (different from) that of the given terminal.

$$G_{[\ldots]}(d_w) = A_{[\ldots]} \exp\{-d_w^2/[s_{[\ldots]}\Phi(k)]^2\}$$

where $\Phi(k) = 0.0015k + 0.4$. The value for $A_{\text{Space}} = 100$, $s_{\text{Space}} = 2.5$; $A_{\text{M/P}} = 30$, $s_{\text{M/P}} = 8$; $A_{\text{Pol,same}} = -2.5$, $s_{\text{Pol,same}} = 6$; $A_{\text{Pol,diff}} = 15$, $s_{\text{Pol,diff}} = 8$; $A_{\text{Eye,same}} = -4$, $s_{\text{Eye,same}} = 6$; $A_{\text{Eye,diff}} = 20$, $s_{\text{Eye,diff}} = 8$. For optic disk "ghost" terminals, $E_{\text{Corr}} = \Sigma G_{\text{Space}}(d_w)$.

$$E_{\text{Pos}} = ay^2 + K_g y$$

where $a = 1.5$, and $K_g = -10, -30, -50, -70, -90, -150$, for $g = 1, 2, 3, 4, 5, 6$, respectively. Terminals were given trial moves according to Gaussian probability distribution functions with standard deviations of 3.5 horizontally and 10.5 vertically.

REFERENCES AND NOTES

1. J. H. Kaas, R. W. Guillery, J. M. Allman, *Brain Behav. Evol.* **6**, 253 (1972).
2. ———, *J. Comp. Neurol.* **147**, 163 (1973).
3. The projection of the transition into visual space is roughly a circle centered on the fovea, passing through the blind spot, 17° from the fovea on the horizontal meridian [J. G. Malpeli and F. H. Baker, *ibid.* **161**, 569 (1975)]. Each LGN represents (mainly) the contralateral hemifield, so only contralateral-eye layers map the blind spot.
4. Retinal ganglion cells that project to magnocellular (large soma) or parvocellular (small soma) layers are conventionally referred to as M and P cells, respectively. P cells have color-opponent properties, whereas M cells have broad-band wavelength sensitivity [T. N. Wiesel and D. H. Hubel, *J. Neurophysiol.* **29**, 115 (1966)].
5. J. G. Malpeli, D. Lee, F. H. Baker, *Invest. Ophthalmol. Visual. Sci.* **34**, 812 (1993).
6. P. Rakic, *Science* **214**, 928 (1981).
7. E. Aarts and J. Korst, *Simulated Annealing and Boltzmann Machines* (Wiley, New York, 1989).
8. The basic organization of the primate LGN (most obvious in four-layered regions) is parvocellular layers, dorsal; magnocellular layers, ventral; ipsilateral eye layers, innermost (middle layers); and contralateral eye layers, outermost (most dorsal and ventral) (*1*). In the six-layered region, On and Off P terminals are largely (but incompletely) segregated by layer, with On-dominated layers dorsal to Off-dominated layers [P. H. Schiller and J. G. Malpeli, *J. Neurophysiol.* **41**, 788 (1978); C. R. Michael, *Proc. Natl. Acad. Sci. U.S.A.* **85**, 4914 (1988); but see also A. M. Derrington and P. Lennie, *J. Physiol. (London)* **357**, 219 (1984)]. This stratification may also continue within the merged parvocellular layers in the four-layered region [P. H. Schiller and J. G. Malpeli, *J. Neurophysiol.* **41**, 788 (1978)]. With respect to the link between blind spot and laminar transition, the validity of the simulation does not depend on the assumption of On/Off segregation specifically. A segregation based on any distinction would be sufficient, as long as categories thus formed obeyed the same rules as On/Off terminals.
9. P. O. Bishop, W. Kozak, W. R. Levick, G. J. Vakkur, *J. Physiol. (London)* **163**, 503 (1962); K. J. Sanderson, *Exp. Brain Res.* **13**, 159 (1971).
10. Simulating the blind spot without ghost terminals produced the same results with regard to trapping laminar transitions, but terminals from ipsilateral eye layers intruded deeply into optic disk gaps. To eliminate the possibility that the success of the simulation was related to this unrealistic local thickening of ipsilateral eye layers, we incorporated ghost terminals as place-keepers in the gaps.
11. Allowing movements to higher energy states reduces the chances of trapping the system in a local minimum.
12. The slope of the interaction-distance function is not a critical parameter for obtaining laminar transitions: Logically, it can be arbitrarily close to 1 if the "cooling rate" is sufficiently low. We have obtained the same laminar pattern with smaller slopes and lower cooling rates.
13. The packing density of cells drops monotonically in the rhesus LGN [W. E. Le Gros Clark, *J. Anat.* **75**, 419 (1941)]. Such changes are likely related to the drop in retinal magnification with eccentricity. Perhaps the variations in the complexity of laminar patterns among different species of primates could be accounted for by a single model incorporating realistic magnification functions for each species.
14. The odds of obtaining a capture rate of 56.5% by chance are essentially zero: A Monte Carlo shuffle of gap and transition locations produced not a single case of this capture rate in 10^8 shuffles.
15. Were the cooling rate sufficiently low, natural transitions would all occur at a single location determined by the global energy minimum.
16. The ability of the blind spot to trap transitions did not appear to depend strongly on particulars of the model. Preliminary models often produced incorrect or multiple transitions, including models with constant interaction distances, different algorithms for establishing retinotopy, and different methods of representing the blind spot. Even in these cases, whenever parameters were found that produced a change in laminar pattern, the blind spot tended to trap transitions.

17. We thank K. Akins, D. Cooper, E. Dzhafarov, E. Erwin, J. Geistlinger, J. Juraska, E. Meisami, V. Pavlovic, K. Schulten, S. Tzonev, and T. Weyand for their suggestions. Color graphics were created at the Beckman Visualization Facility. Supported by National Institutes of Health grant EY02695 and National Science Foundation grant DIR91-16763.

9 August 1993; accepted 30 November 1993